JTTEE5 20:121–131
DOI: 10.1007/s11666-010-9590-0
1059-9630/$19.00 © ASM International

Effect of Chemical Compositions and Surface Morphologies of MCrAlY Coating on Its Isothermal Oxidation Behavior

Yong Li, Chang-Jiu Li, Qiang Zhang, Lu-Kuo Xing, and Guan-Jun Yang

(Submitted May 13, 2010; in revised form September 29, 2010)

Chemical composition and surface morphology of MCrAlY coatings are factors which influence the oxidation behavior and the thermal durability of thermal barrier coatings. In this study, Cold-sprayed Ni20Cr10AlY and Ni23Co20Cr8.5Al4.0Ta0.6Y coatings with polished surfaces were employed to study the effect of composition on the oxidation behavior. The cold-sprayed MCrAlY coatings at the as-sprayed and shot-peened surface conditions, along with the low pressure plasma-sprayed MCrAlY coating with sputters adhered weakly on the surface, were employed to investigate the effects of surface morphologies of MCrAlY coatings on their oxidation behavior. Cold-sprayed Ni20Cr10AlY coating exhibited a two-stage oxidation behavior and a higher TGO growth rate than that of the cold-sprayed Ni23Co20Cr8.5Al4.0Ta0.6Y coating at the rapid growth stage. After 10-h oxidation, the TGO on the as-cold-sprayed coating surface was mainly constituted by Al_2O_3, while the TGO on the coating surface attached with sputters was composed of Al_2O_3 and Cr/Ni-oxides. After 500-h oxidation, Cr_2O_3 and porous spinel appeared in the TGO on the surface of the as-cold-sprayed coatings with different compositions. The growth of Cr/Ni-oxides was attributed to the Al depletion. The content of spinel decreased on the cold-sprayed NiCrAlY with a shot-peened surface compared with the as-sprayed coating.

Keywords cold spray, composition, low pressure plasma spraying, MCrAlY coating, oxidation behavior, surface morphology

1. Introduction

Durability and performance of advanced gas turbines for aircraft and industrial engine applications have been improved with the application of thermal barrier coatings (TBCs) to high pressure turbine airfoils (Ref 1-4). Their application can reduce the in-service surface temperature of the underlying superalloy blades (Ref 1, 2). Thermal barrier coatings are composed of superalloy blade, MCrAlY bond coat, yttria-stabilized zirconia (YSZ) coating, and a thermally grown oxide (TGO) which grows at the interface between the bond coat and the YSZ coating (Ref 1, 5-8). The uniformity along the interface and the constituents of TGO are significantly influenced by the surface morphology of the bond coat before YSZ deposition (Ref 9, 10).

Either atmospheric plasma spraying (APS) or electron beam physical vapor deposition (EB-PVD) is used to deposit YSZ coating as the thermal insulator (Ref 1, 7, 8, 11). The demands for bond coat surface condition are different when each of the above mentioned YSZ deposition methods is employed. With APS, an undulating metal/ceramic interface is required for a better interlocking adhesion. Such interface morphology produces the out-of-plane stresses responsible for in-service failure (Ref 10). The out-of-plane stress due to the undulating bond coat surface induces the spalling between the TGO and the bond coat at the undulation crest (Ref 12, 13), and promotes the formation of local accumulated TGO protrusion (Ref 14). In contrast to the APS, the bond coat surface can be smooth before deposition when EB-PVD is applied to deposit YSZ coating. It was reported (Ref 9, 15-18) that TGO usually penetrates into bond coat when a smooth bond coat surface is applied to EB-PVD TBCs. The difference of TGO growth behavior on the MCrAlY bond coat with an undulation surface from a smooth surface indicates the important effect of the surface morphology of bond coat on TGO growth and evolution.

The influence of bond coat surface morphology on its oxidation behavior and even the TBCs durability was less experimentally investigated because of the difficulty to control its surface morphology. The bond coats at a

This article is an invited paper selected from presentations at the 2010 International Thermal Spray Conference and has been expanded from the original presentation. It is simultaneously published in *Thermal Spray: Global Solutions for Future Applications, Proceedings of the 2010 International Thermal Spray Conference*, Singapore, May 3-5, 2010, Basil R. Marple, Arvind Agarwal, Margaret M. Hyland, Yuk-Chiu Lau, Chang-Jiu Li, Rogerio S. Lima, and Ghislain Montavon, Ed., ASM International, Materials Park, OH, 2011.

Yong Li, Chang-Jiu Li, Qiang Zhang, Lu-Kuo Xing, and **Guan-Jun Yang**, State Key Laboratory for Mechanical Behavior of Materials, School of Materials Science and Engineering, Xi'an Jiaotong University, Xi'an 710049, Shaanxi, People's Republic of China. Contact e-mail: licj@mail.xjtu.edu.cn.

polished surface condition are used for YSZ deposition by EB-PVD. When the surface roughness of the MCrAlY bond coat changed from 3.76 to 0.82 μm, the lifetime of the EB-PVD deposited TBCs increased from about 500 h (1000 cycles) to 700 h (1400 cycles) (Ref 19). Hesnawi et al. (Ref 10) reported that the bond coat with a shot-peened surface shows a better oxidation resistance as compared to a polished surface. α-Al_2O_3 and θ-Al_2O_3 are developed on the polished surface. Only α-Al_2O_3 is detected on the shot-peened surface after the pre-oxidation treatment. The results reported by Gil et al. (Ref 9) showed that the as-sprayed NiCoCrAlY surface after the oxidation at 1100 °C become different in the morphology of oxide scale at the concave area from the convex surface area. The convex surface areas exhibited relatively thin alumina scale and frequent spinel-formation on the top of the scale. In contrast, on the concave surfaces, the scale is thicker with hardly any spinel formed on the top of the scale. The surface morphology also influences the microstructure change of bond coat during oxidation. The cross-sectional microstructure images reported by Gil et al. (Ref 9, 20) and Rabiei and Evans (Ref 21) showed that the β-NiAl depletion zone in LPPS bond coat is much thicker beneath the convex area than that beneath the concave area.

The surface morphology of MCrAlY bond coat is influenced by its deposition method and the melting state of feed-stock powder particles during deposition. Atmospheric plasma spraying (APS), high-velocity oxygen-fuel spraying (HVOF) and low pressure plasma spraying (LPPS) have been employed to deposit MCrAlY coating (Ref 22, 23). Generally, the coatings by the above mentioned thermal spray processes are deposited through the stacking of spray particles in a completely or partially melted state. The rough surface of the MCrAlY coating will cause splashing on impact, which results in the adherence of sputters. Our previous report (Ref 24) showed that the sputters on the MCrAlY bond coat surface influence significantly the composition of TGOs and consequently the thermal fatigue behavior.

Cold spraying is also being investigated to deposit MCrAlY coating (Ref 24-27). A cold-sprayed coating is formed through the plastic deformation upon the impact of sprayed particles at a temperature well below the melting point of the spray material, which makes the cold spraying become an alternative method to deposit a dense MCrAlY bond coat in thermal barrier coatings without oxidation (Ref 24-28). The simulation results reported by Li et al. (Ref 29) and Grujicic et al. (Ref 30) indicate that the intensive deformation occurs mainly at the bottom of a particle, while the upper surface of an impacting particle may experience less deformation. The simulation result is supported by the images of the cold-sprayed MCrAlY coating surface reported in Ref 31 and 32. Accordingly, the particles deposited on the top surface of the MCrAlY coating may maintain their original powder particle surface condition. This fact suggests that the surface morphology of the cold-sprayed MCrAlY coating is possibly much different from the thermally sprayed ones. Our previous study (Ref 24) indicated that the MCrAlY bond coats deposited by cold spraying and LPPS exhibited different surface morphologies which led to the different thermal fatigue behavior of TBCs. In order to further clarify the influence of the surface morphology of the MCrAlY coating on the oxidation behavior, besides the surface conditions at the as-sprayed state reported in the previous study (Ref 24), the surfaces of the cold-sprayed MCrAlY coatings was subjected to polishing and shot-peening treatment before oxidation and the influence of the surface morphologies of the MCrAlY coatings on its oxidation behavior was investigated. Moreover, the influence of the MCrAlY coating composition on the TGO growth behavior was also investigated.

2. Materials and Experimental Procedures

2.1 Cold Spraying of MCrAlY Coating

Inconel 738 superalloy machined to the dimensions of ∅ 16 × 3 mm was used as the substrate. Ni-20Cr-10Al-1Y (Fig. 1a) and Ni-23Co-20Cr-8.5Al-4.0Ta-0.6Y (Fig. 1b) powders with $d_{0.5}$ equal to 37.4 and 23 μm, respectively,

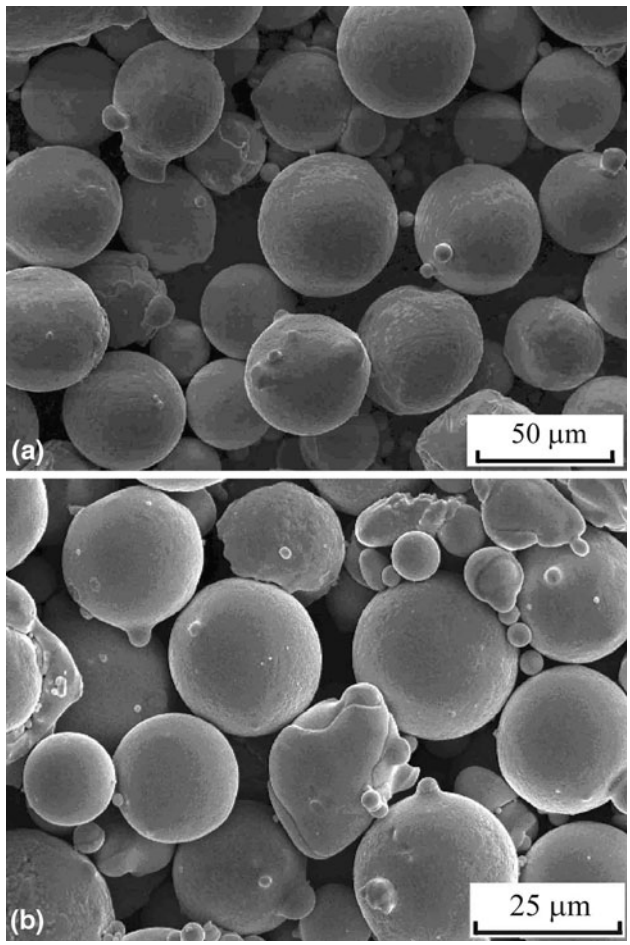

Fig. 1 Morphologies of starting powders for the cold spraying of MCrAlY coating: NiCrAlY (a); NiCoCrAlTaY (b)

were used as the feedstocks for cold spraying. The coatings were deposited using the cold spray system (CS-2000) developed in Xi'an Jiaotong University, China. During cold spraying, helium was employed as the accelerating and powder feeding gas operating at 2.0 and 2.6 MPa, respectively. The temperature of the accelerating gas was maintained at 580 ± 20 °C during cold spraying. The spray gun traversed at a speed of 150 mm/s and the spray distance was kept at 20 mm.

2.2 Preparation of LPPS MCrAlY Coating

With LPPS, a commercial plasma spray system (GTV-MFP1000 LPPS system) was employed to deposit NiCoCrAlTaY coating. The LPPS coating was deposited at a chamber pressure of 0.008 MPa charged with Ar in Guangzhou Research Institute of Non-ferrous Metals, China. The arc current and voltage during LPPS were 625 A and 65 V, respectively. Argon was used as the primary plasma gas operating at a flow of 60 slpm. Hydrogen was used as the secondary plasma gas operating at a flow of 4.5 slpm. The spray distance was 250 mm.

2.3 Surface Preparation of MCrAlY Coating

The surfaces of MCrAlY coating were prepared to the following different conditions: as-sprayed surface (LPPS and cold spraying), polished surface (cold spraying), shot-peened surface (cold spraying). The surface polishing was carried out using 1.5 μm diamond polishing agent. The shot-peening treatment was carried out using a commercial shot-peening machine (MT1500) by glass beads of a diameter of 0.3 mm at a working distance of 150 mm between the nozzle and the coating surface. The pressure was 0.3 MPa during shot-peening.

2.4 Oxidation Experiment

The coatings at the as-sprayed, polished, and shot-peened conditions were subjected to the isothermal oxidation at 1000 °C in air atmosphere. The details of the oxidation experiment conditions are listed in Table 1. The coatings with a polished surface being used for the investigation of the effect of MCrAlY composition on the oxidation behavior were positioned in the furnace once the set temperature was reached, and then allowed to soak for durations of 1, 2, 4, 10, 50 and 200 h, respectively, to remove the effect of slow heating process. To study the effect of surface morphologies on the oxidation behavior, the cold-sprayed coatings at the as-sprayed and shot-peened surface conditions and LPPS coating at the as-sprayed surface condition were soaked in static atmospheric air at 1000 °C for duration of 10 and 500 h. After the oxidation for the given periods, the samples were moved out from the furnace and were cooled down to room temperature. Ni-electroless plating was employed to deposit a layer of Ni on the surface of the oxidized samples to protect the TGO scale from spalling during the metallographic sample preparation. After the polishing of sample cross-sections, the thickness of TGO was examined through scanning electron microscopy (SEM, VEGA II-XMU, TESCAN, Czech) in order to investigate the oxide growth rate on the coatings with different compositions, and the effect of the surface morphologies of the coating on the TGO growth. X-ray diffraction (XRD, Rigaku D/max-2400) and EDS were employed to characterize the composition of TGO.

Table 1 Surface conditions of the MCrAlY bond coat samples and oxidation conditions employed

Surface conditions	Cold spraying		LPPS
	NiCrAlY	NiCoCrAlTaY	NiCoCrAlTaY
Polished	1, 2, 4, 10, 50, 200 h	1, 2, 4, 10, 50, 200 h	
As-sprayed	500 h	10, 500 h	10 h
Shot-peened	500 h		

3. Results and Discussion

3.1 Characterization of MCrAlY Coating Surface Morphology

Figure 2 shows the typical surface morphology of cold-sprayed NiCoCrAlTaY coating. Some large partially deformed spherical particles were observed on the as-sprayed coating surface, as shown in Fig. 2(b). Evidently, these large spherical particles almost retained their original powder morphology. The surface of these particles was smooth with little deformation, as shown in Fig. 2(b). Moreover, the cross-sectional microstructure of the cold-sprayed coating shows that such particles adhered well to the sub-layer, as shown in Fig. 2(c).

The surface morphology of the NiCoCrAlTaY coating deposited by LPPS is shown in Fig. 3(a). Large spherical particles deposited by partially melted spray particles were recognized from the surface of the LPPS coating. A close examination revealed that substantial small particles with a diameter less than 1 μm attached to the surface of these large particles, which makes the surface of spherical particles less smooth (Fig. 3b) compared with the surface of these particles (Fig. 2b) on the as-cold-sprayed coating surface. Such characteristics of the surface morphology have been reported in our previous report (Ref 24). Possibly such surface morphological feature results from the splashing of the melted fraction of the partially melted spray particles upon their impacts during LPPS.

Some large near spherical particles were contained on the surfaces of both the LPPS and the cold-sprayed coating. However, those particles were deposited by different deposition mechanisms. The large spherical particles appeared on the LPPS coating surface were recoated by the sputters which weakly adhered to the underlying particles and increased the coating surface areas. On the other hand, no such phenomenon was observed on the cold-sprayed coating surface. To less extent, part of the particle area on the surface of cold-sprayed coating was impacted by rebound particles, resulting in a concave profile, as shown in Fig. 2(b).

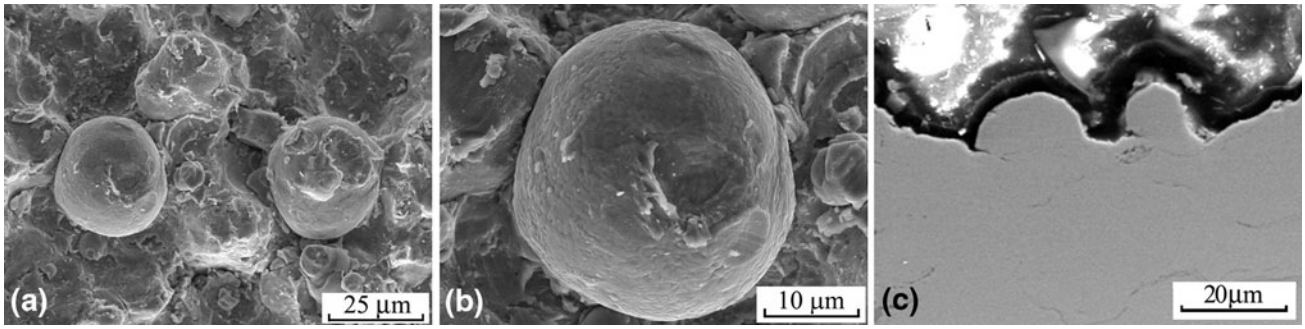

Fig. 2 Surface morphology of the cold-sprayed NiCoCrAlTaY coating (a); the detailed surface morphology of spherical particle observed at a higher magnification (b); cross-sectional microstructure of the MCrAlY coating (c)

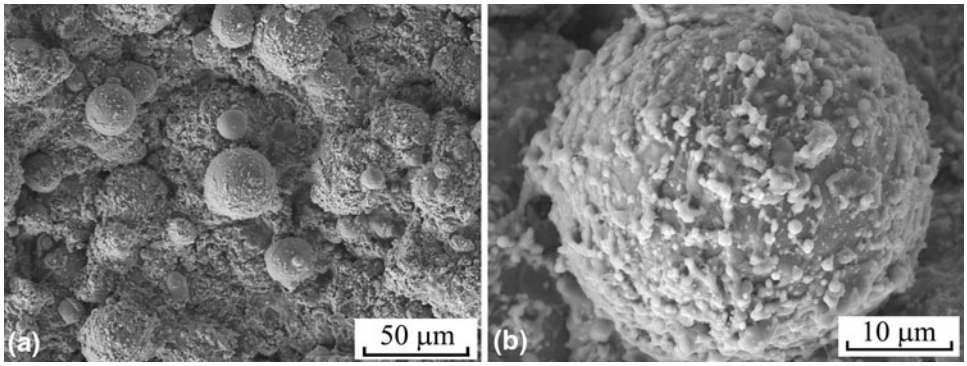

Fig. 3 Surface morphology of LPPS NiCoCrAlTaY coating (a); detailed indication of sputters on the LPPS coating surface (b)

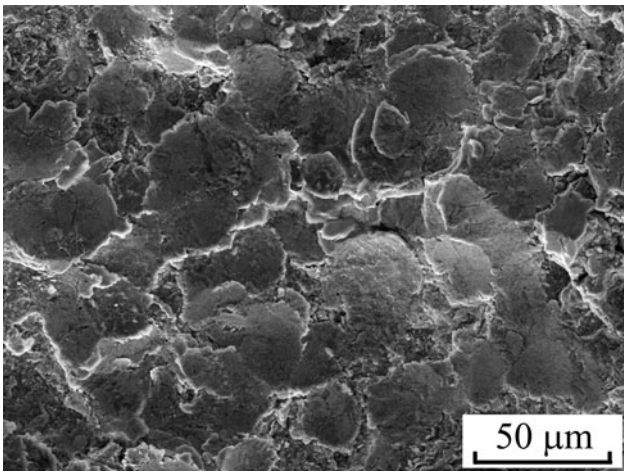

Fig. 4 Surface morphology of the cold-sprayed NiCrAlY coating after shot-peening

The application of shot-peening to the cold-sprayed MCrAlY coating modified the coating surface morphology. The spherical particles on the as-sprayed coating (see Fig. 2a) disappeared after the shot-peening (Fig. 4). Local flat surface and some extrusion were formed because of the impacting during the shot-peening treatment. The shot-peening may also wipe off some particles that were much weakly bonded to the sub-layer.

3.2 Effect of MCrAlY Coating Compositions on the Oxidation Behavior

Figure 5 shows the phase compositions of the TGOs formed on the polished surface of two types of cold-sprayed MCrAlY coatings with different compositions after 1 and 200 h oxidation. The TGOs formed on both the cold-sprayed MCrAlY coatings with a polished surface exhibited the same compositions after 1 h oxidation. Only α-Al_2O_3-based TGO was formed on both the coatings. A little fraction of $NiAl_2O_4$ was formed on the NiCrAlY coating after 200 h oxidation, while only α-Al_2O_3-based TGO was observed on the NiCoCrAlTaY coating after 200 h oxidation. Figure 6 shows the cross-sectional microstructure of the TGOs formed on two cold-sprayed coatings. After 1 h oxidation, the average TGO thicknesses on the NiCrAlY and the NiCoCrAlTaY coatings reached 0.55 and 0.21 μm, respectively (Fig. 6a, b). After 200 h oxidation, 2.3 μm versus 1.4 μm thick TGO (Fig. 6c, d) grew on the surface of the cold-sprayed NiCrAlY and NiCoCrAlTaY coatings, respectively. Y-Al oxides in bright contrast (as marked by arrows in Fig. 6c) were also observed in the TGO of NiCrAlY coatings after 200 h, while it was too little to be detected by x-ray diffraction. These results show that an uniform α-Al_2O_3-based TGO scale was primarily formed on both the coatings with the polished coating surfaces.

Figure 7 shows the dependence of the oxide thickness on two cold-sprayed MCrAlY coatings with the surface

polished on the oxidation time. The cold-sprayed NiCoCrAlTaY coating exhibited a lower TGO growth rate than the NiCrAlY coating. Evidently, the TGO growth on the NiCoCrAlTaY coating followed a parabolic rule with the oxidation time:

$$h = 0.103t^{1/2} \quad \text{(Eq 1)}$$

where t is the exposure time in hours and h is the thickness of TGO in micrometers. Moreover, the oxidation of the NiCrAlY coating could be divided into two stages: a rapid growth stage and a steady oxidation stage. During the rapid growth stage, the parabolic growth constant K_p is 0.365 μm/h^2. This means that the growth rate of TGO on the cold-sprayed NiCrAlY coating is increased by a factor of 3.5 compared to the cold-sprayed NiCoCrAlTaY coating. The rapid growth occurred for about 10 h. After the rapid growth model, the TGO growth occurred in a fashion as that observed for NiCoCrAlTaY, which is referred to as the steady oxidation model. During the steady oxidation stage, the TGO growth rate K_p was reduced to 0.104 μm/h^2, close to that of the NiCoCrAlTaY coating.

Seo et al. (Ref 33) reported that the vacuum plasma sprayed (VPS) NiCrAlY coating showed the highest

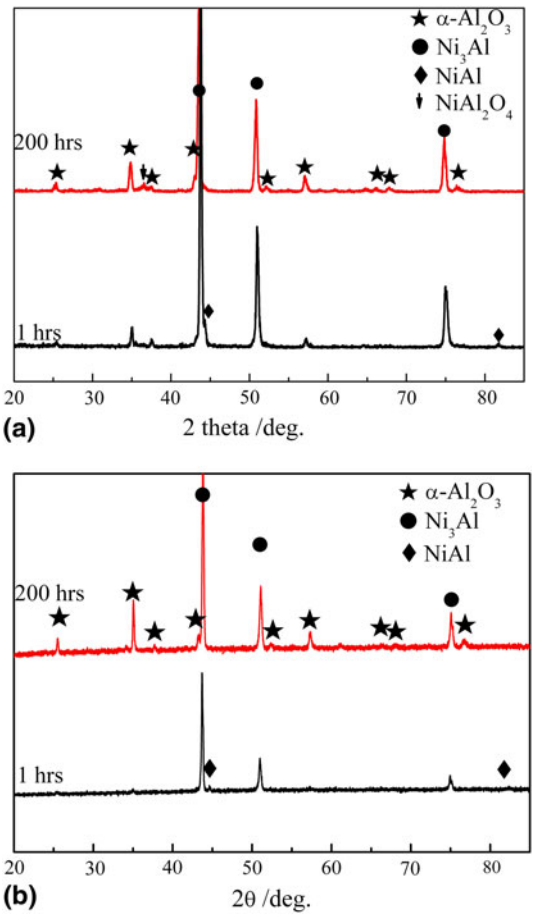

Fig. 5 XRD patterns to show the phase compositions of TGO grew on the cold-sprayed coatings at the surface polished conditions with NiCrAlY composition (a) and NiCoCrAlTaY composition (b) after different times of oxidation

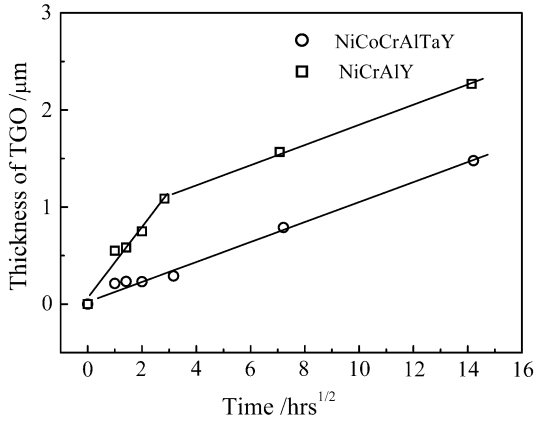

Fig. 7 Thickness of TGO against the oxidation time for two cold-sprayed MCrAlY coatings

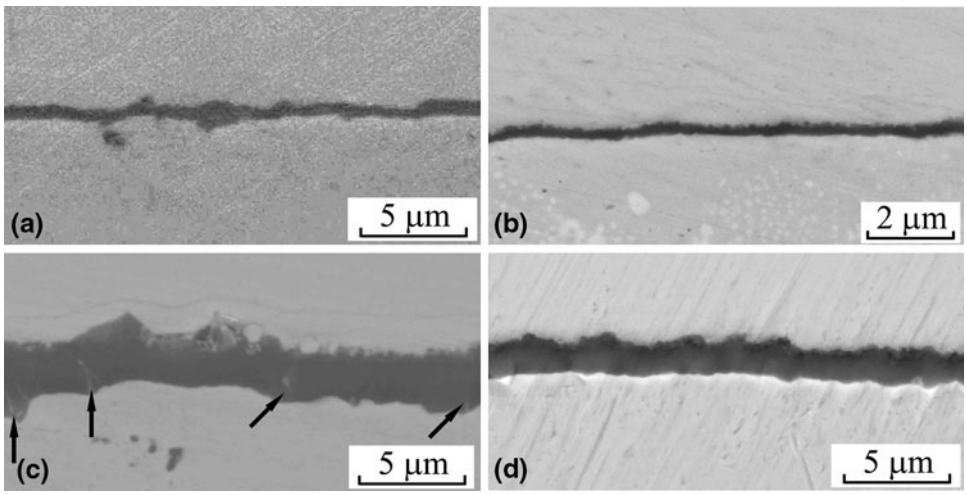

Fig. 6 Cross-sectional microstructure of TGO formed on the polished surfaces of the cold-sprayed coatings: (a) NiCrAlY, 1 h; (b) NiCoCrAlTaY, 1 h; (c) NiCrAlY, 200 h, Y-Al oxides marked by arrows; (d) NiCoCrAlTaY, 200 h

oxidation rate among four VPS MCrAlY coatings (M = CoNi (8%), Co (13%), NiCo (13%), Ni (11%), percentage in the bracket stands for the Al content of each powder) and a two-stage TGO growth behavior similar to the present study. This two-stage oxidation behavior was also observed for FeCrAlY coating (Ref 34).

Although it was suggested (Ref 33) that the porosity in the NiCrAlY coating was responsible for the two-stage oxidation behavior, the characterization of the present cold-sprayed coating as shown in Fig. 2(c) suggested the formation of the NiCrAlY coating with a dense microstructure. The two-stage oxidation behavior observed in the present study is possibly associated to the surface morphology evolution of the Al_2O_3-based TGO. Figure 8 shows the surface morphology of the TGOs formed on the polished NiCrAlY surface after 1 and 200 h oxidation. It was found that the TGO exhibited a relative rough surface after 1 h oxidation and rod-like oxides were observed in the TGO. The rod-like oxide, resulting in the formation of a rough surface, is possibly because of the preferential growth of the transient oxide such as θ-Al_2O_3 at the early oxidation stage during temperature ramping. θ-Al_2O_3 in the shape of needle or rod is preferentially formed at a temperature range lower than 940 °C (Ref 35). The preferable growth of the transient oxide results in a high local growth rate at very early oxidation stage, which results in a high apparent TGO growth rate. Investigations (Ref 1, 27) indicated that the surface morphology of Al_2O_3-based TGO does not change after the transformation of the transient θ-Al_2O_3 to the stable α-alumina. With the growth of α-Al_2O_3 at a temperature of 1000 °C, the thickness of the TGO tends to become uniform because the length of diffusion path of elements is proportional to the TGO thickness, which possibly leads to the reduction of the apparent TGO growth rate with the progressing of oxidation. Accordingly, after long time oxidation such as 200 h, the rod-like oxide was not observed and the surface of TGO becomes less rough.

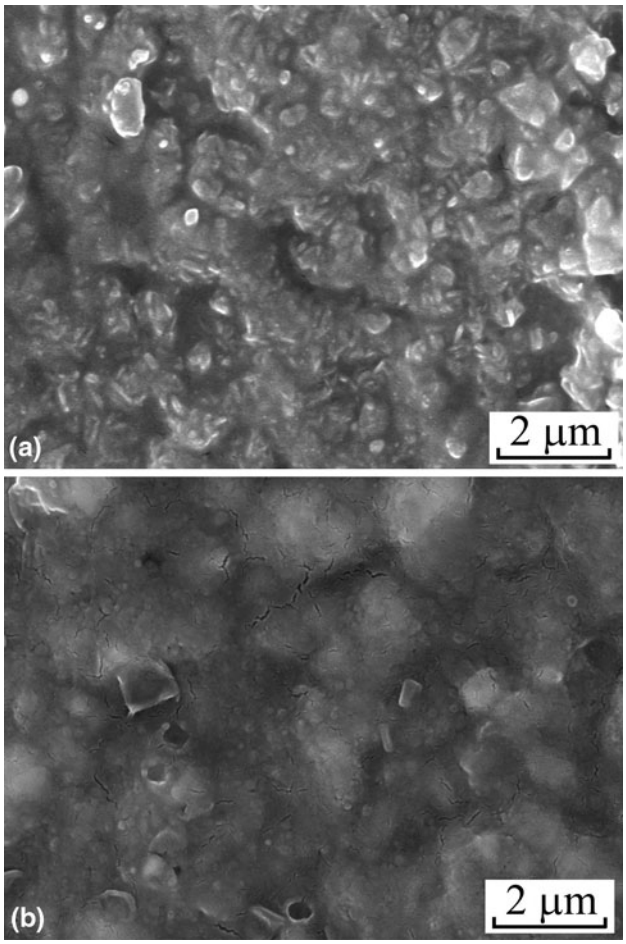

Fig. 8 Surface morphology of TGOs evolved on the polished surface of the cold-sprayed NiCrAlY coating after 1 h oxidation (a) and 200 h oxidation (b)

3.3 Effect of Surface Morphologies on the TGO Composition

3.3.1 Features of TGOs Formed on the As-Cold-Sprayed and LPPS Coating Surfaces. The distinct TGO compositions (Fig. 9, 10) were observed for the coatings with the surfaces formed by different deposition mechanisms. Table 2 shows the EDS point analysis results for the composition of the TGO (Fig. 9) on the as-cold-sprayed NiCoCrAlTaY coating surface. Al and O elements dominated the TGO composition. The content of O element was underestimated because of its low atomic weight. The appearance of Ni, Co, Cr and Y elements in the EDS result is attributed to the small TGO thickness compared to the interaction volume between the electron beam and the target material. It can be confirmed that the TGO with a black contrast under the BEI mode was Al_2O_3. After 10 h oxidation, only Al_2O_3 formed on the MCrAlY coating surface. The thickness of the Al_2O_3-based TGO was uniform, as shown in Fig. 9. Because of the good adhesion of particles exposed on the cold-sprayed coating surface with its sub-layer (Fig. 2c), during

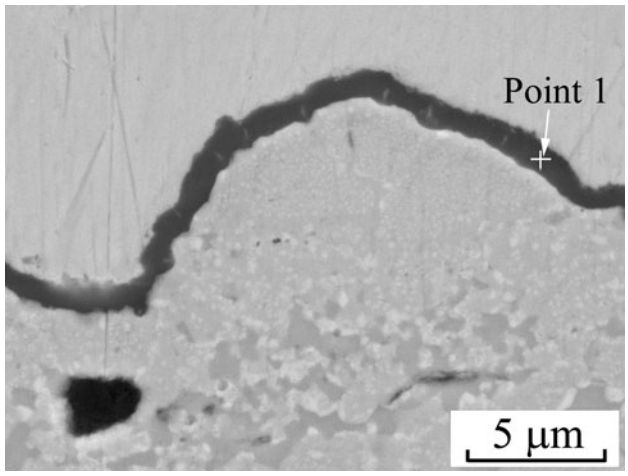

Fig. 9 Microstructure of TGO on the surface of the as-cold-sprayed NiCoCrAlTaY coating after 10 h exposure in air and the indication of the position for EDS point analysis for the confirmation of TGO composition

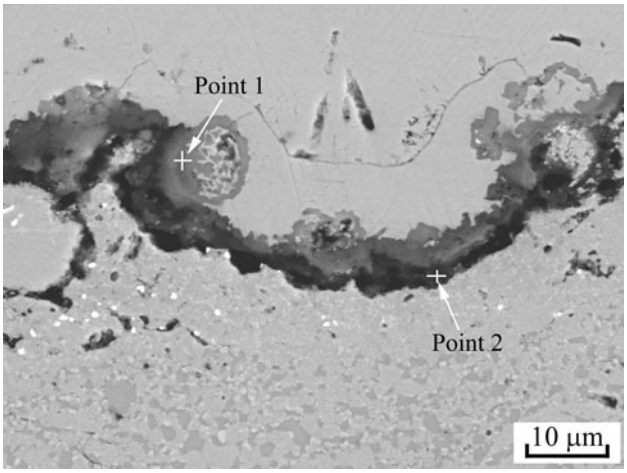

Fig. 10 Microstructure of TGO on the as-sprayed surface of LPPS NiCoCrAlTaY coating with sputters attached after 10 h exposure in air and the EDS points used for the confirmation of TGO composition

Table 2 TGO compositions in Fig. 9 by EDS point analysis

Point in Fig. 9	Ni	Co	Cr	Al	Y	O
Point 1, at.%	5.17	2.51	3.51	67.87	1.28	19.65

Table 3 TGO composition results in Fig. 10 by EDS analysis

Points in Fig. 10	Ni	Co	Cr	Al	Y	O
Point 1, at.%	38.10	16.50	24.55	14.25		11.80
Point 2, at.%	10.64	0.50	1.41	64.17	2.56	20.72

oxidation, the rapid Al diffusion without barrier promoted the growth of the Al_2O_3-based TGO.

On the other hand, with the surface of the LPPS NiCoCrAlTaY coating covered with sputters, the compositions of TGO became complex (Fig. 10) as reported in the previous paper (Ref 24). The results of the EDS analysis (as listed in Table 3) indicate that the TGO exhibited different compositions at different locations of the TGO. The EDS analysis results at two points indicate that Cr/Ni-rich TGO formed on the Al_2O_3 layer (Fig. 10). The high Ni content (10.64 at.%) in the point 2 is possibly attributed to the limited thickness of the Al_2O_3-based TGO scale compared with the effective spot diameter (2.74 μm) of the electron beam during EDS. The average thickness of TGO was about 8 μm which was much thicker than that of the TGO formed on the cold-sprayed coating surface without sputters. When compared with the cold-sprayed coating, splashing during LPPS led to the modification of the deposited particle surface by sputters. Those sputters weakly adhered to the surface of the LPPS coating. Moreover, sputters increase the surface area of MCrAlY coating. Consequently, an increased surface area results in the rapid consumption of Al during oxidation. It has been reported (Ref 36, 37) that, compared to other oxides triggered by the oxidation, Al_2O_3 preferably forms at MCrAlY coating surface, since the oxidation of Al requires the least oxygen pressure and the lowest Gibbs free energy of formation than other metal elements, such as Ni, Cr, etc. The rapid consumption of Al during the oxidation requires its diffusion supply from underlying splats/particles. The weak bonding between the sputter and the underlying splat in LPPS coating limits or delays the diffusion of Al to sputter surface after Al depletion occurred in the sputter. Cr/Ni oxides grow fast due to the diffusion of Ni, Cr elements through Al_2O_3 grain boundaries in spite of the formation of Al_2O_3 scale underlying (Ref 24, 38), leading to the formation of Cr/Ni oxides on the surface of sputters.

3.3.2 The Characteristics of TGO on the As-Sprayed Surface and Shot-Peened Surface. In order to examine the oxidation behavior after a long time (500 h) exposure, the cold-sprayed NiCrAlY coatings at the as-sprayed and shot-peened conditions were employed. With the as-sprayed coating, both the dense oxide and porous oxide (as marked by the white arrows in Fig. 11a) formed on the surface. According to the TGO morphology (Ref 25, 33), image contrast taken in the BEI (SEM) mode and the EDS elements mapping results on the cross-section (Fig. 11b) of the oxidized coating, it was considered that the porous oxides is spinel. The dense TGO exhibited a double layer structure, within which the outer layer was Cr_2O_3, and the inner TGO near to the NiCrAlY coating was Al_2O_3, as shown in Fig. 11(b). On the other hand, the application of the shot-peening treatment induced a local flat surface, and the porous oxides disappeared at these places (Fig. 12a). However, at the surface areas less flat, the porous oxides were also observed, as shown in Fig. 12(b), but its content at the whole surface was largely reduced (Fig. 12a). The shot-peening treatment seems only effective to reduce the porous spinel. The TGO on the shot-peened surface still exhibited a double layer structure and was composed of Al_2O_3 at the inner layer and Cr/Ni oxides at the outer layer, as shown by the EDS line analysis in Fig. 12(c).

In order to understand the formation of the Cr/Ni-oxides on the NiCrAlY coating, the cold-sprayed NiCoCrAlTaY coating was also oxidized for 500 h (Fig. 13a). Firstly, the TGO (3 μm thick) formed on the NiCoCrAlTaY coating was thinner than that on the NiCrAlY coating (7 μm). Secondly, the Cr/Ni-oxides occasionally formed at the outer layer of the TGO, as marked by black arrows in Fig. 13(b). The comparison of the oxidation behavior of two cold-sprayed MCrAlY coatings suggests that Cr/Ni-oxides still formed on both the cold-sprayed MCrAlY coatings after long time (500 h) oxidization, although a continuous and dense Al_2O_3-based TGO formed during the earlier time of oxidization. However, the distribution of Cr/Ni oxides at coating surface indicated that the time when Cr/Ni-oxides initially appeared was different and determined by the coating composition and the Al depletion rate. With the NiCoCrAlTaY coating, the 500 h oxidation possibly corresponds to the onset of the Cr/Ni-oxides growth. On the other hand, with the NiCrAlY

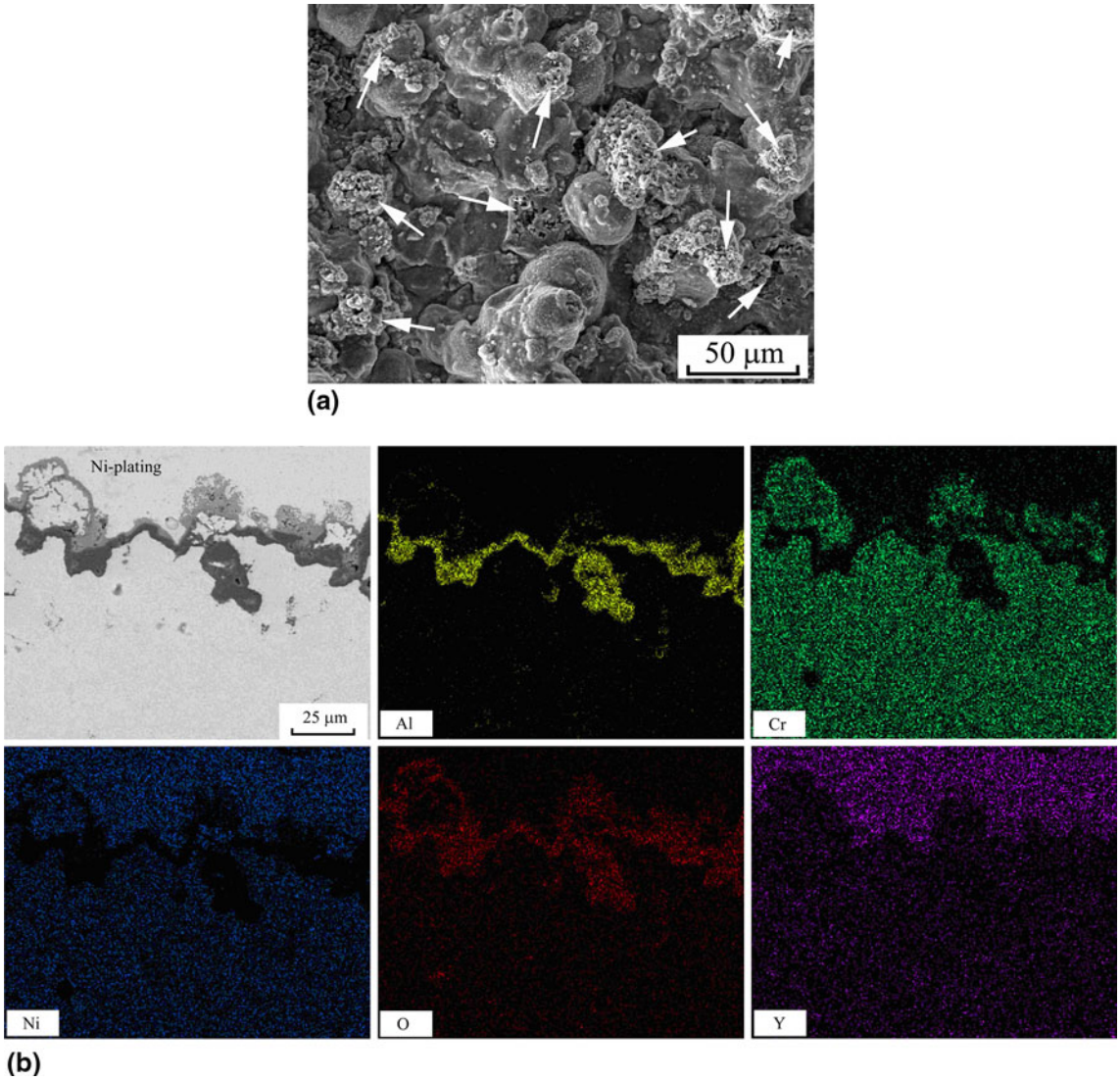

Fig. 11 Surface morphology of TGO formed on the as-sprayed NiCrAlY coating surface after 500 h oxidation (a). Porous oxides (white arrows) were formed on the surface; cross-sectional microstructure of TGO formed on the as-sprayed coating surface after 500 h oxidation and elements mappings (b)

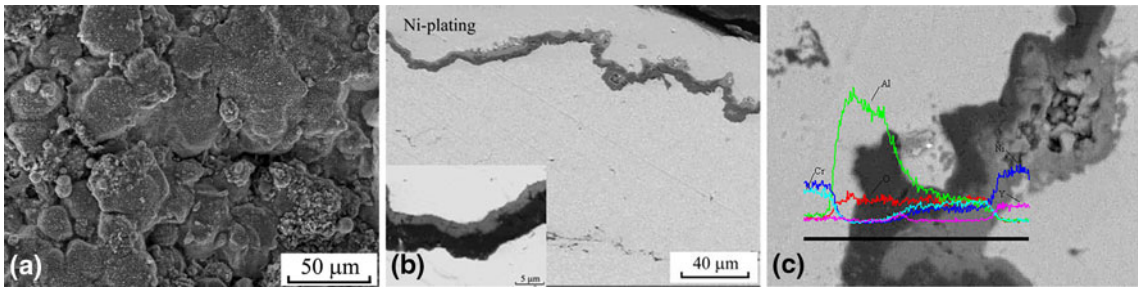

Fig. 12 Surface morphology of TGO formed on the shot-peened NiCrAlY coating surface (a) after 500 h oxidation; cross-sectional microstructure of TGO formed on the shot-peened coating surface after 500 h oxidation (b). EDS line analysis results along the TGO indicating the TGO compositions after 500 h oxidation (c)

coating, the 500 h oxidation corresponded to the excessive growth of the Cr/Ni-oxides. When Al is depleted in the zone near the NiCrAlY coating surface to a certain extent, the continuous formation of α-Al_2O_3 would terminate (Ref 39). In this case, Cr, Ni and Co might diffuse through α-Al_2O_3 scale to the surface of the α-Al_2O_3 layer to form

Cr_2O_3 and $(Ni,Co)(Cr,Al)_2O_4$ spinel (Ref 1) on the condition that the duration time was sufficient. The diffusion of Cr in Al_2O_3 coating is confirmed by Dressler et al. (Ref 40) who prepared a Al_2O_3 coating on the surface of Inconel-718 supperalloy by sol-gel method, and a layer of Cr_2O_3 layer grows at the outside of alumina coating after a long oxidation duration. In fact, the diffusion of Al, Cr, Ni and Co elements in the Al_2O_3 scale was persisting from the beginning of oxidation to the end. The initially formed Al_2O_3-based TGO is due to the low Gibbs free energy of Al_2O_3 formation (Ref 38, 41, 42). In other words, it is more thermodynamically favorable for the Al_2O_3 rather than the Cr/Ni oxides to form. However, after sufficiently long duration of oxidation, Al depletion occurs in the region beneath the surface of coating owing to a reduction of the amount of β-NiAl phase (Ref 43). At the initial 10 h, no Cr/Ni oxides (Fig. 9) were observed at the as-sprayed surface of the cold-sprayed NiCoCrAlTaY coating, while they formed at the top of TGO after the long time oxidation. This fact indicates that Ni and Cr elements diffused to the surface of the alumina scale and formed the Cr/Ni oxides. Tang et al. (Ref 38) also reported that the Cr/Ni oxides formed at the outer layer of Al_2O_3-based TGO after 24 h oxidation at 1000 °C due to the diffusion through alumina scale, while they are absent after 1-h oxidation. Excessive Al depletion even leads to the formation of $NiAl_2O_4$ at the expense of Al_2O_3 when thermodynamic conditions are satisfied according to the following reaction:

$$3Ni + 4Al_2O_3 = 3NiAl_2O_4 + 2Al \quad \text{(Eq 2)}$$

The Al_2O_3 consumption may lead to the thickness reduction of Al_2O_3 scale under the porous spinel, which is previously observed (Ref 43), as shown in Fig. 11(b). The Cr/Ni oxides at the outer-layer of TGO are not an uncommon, and many investigations (Ref 23, 30, 36, 41, 44, 45) reported the same oxidation results.

Compared with the NiCoCrAlTaY coating, Al depleted faster in the NiCrAlY coating due to high oxidization rate of the NiCrAlY coating, which induced the earlier formation of the Cr/Ni-oxides. The Al depletion zone extended to the whole thickness of the NiCrAlY coating (Fig. 11b), and no β-NiAl phase could be observed in the NiCrAlY coating after 500-h oxidation. While with the NiCoCrAlTaY coating, the thickness of β-NiAl depletion zone was in the range of 30-40 μm which was less than half of the coating thickness (Fig. 13a). The thickness of β-NiAl depletion zone is consistent with the effect of Al depletion resulting in the formation of Cr/Ni-oxides.

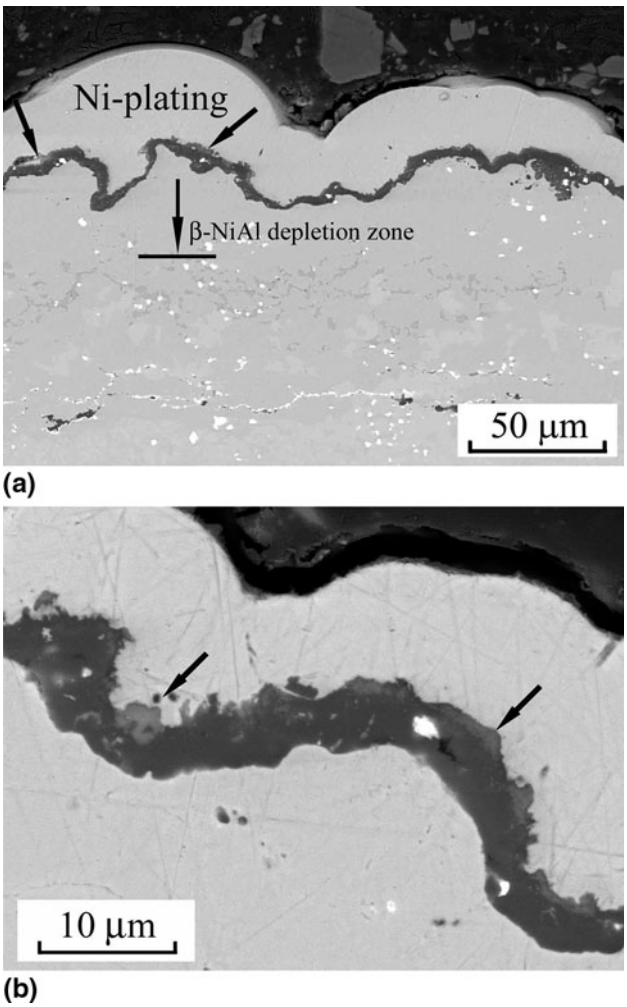

Fig. 13 The cross-sectional microstructures of NiCoCrAlTaY coating (a) and detailed indication of TGO (b) after 500-h oxidation, showing the formation of Cr/Ni oxides (marked by black arrows) at the out-layer of TGO after 500 h oxidation

4. Conclusions

The effects of chemical compositions and surface morphologies of the MCrAlY coating on the TGO growth were investigated using Ni23Co20Cr8.5Al4.0Ta0.6Y and Ni20Cr10AlY as the starting powders. The polished surfaces were employed to study the effect of the composition on the oxidation behavior. The cold-sprayed MCrAlY coatings, under the as-sprayed and shot-peened surface conditions along with low pressure plasma-sprayed MCrAlY coating with sputters adhered weakly on the surface, were employed to investigate the effect of surface morphologies of MCrAlY coatings on the oxidation behavior. The surface of the particles on the cold-sprayed MCrAlY coating surface presented a smooth and spherical configuration similar to that of the original powder surface morphology. The surface of particles on the LPPS coating surface was roughen by the attachment of sputters. The different compositions and surface conditions led to remarkably different oxidation behavior. Cold-sprayed Ni20Cr10AlY coating exhibited a two stage oxidation behavior and a higher TGO growth rate than that of the cold-sprayed Ni23Co20Cr8.5Al4.0Ta0.6Y coating at the rapid growth stage. The growth of the TGO on the cold-sprayed Ni23Co20Cr8.5Al5.0Ta0.6Y coating followed a parabolic rule. The TGO on the as-cold-sprayed MCrAlY

coating surface was constituted by Al_2O_3 after 10-h oxidation. After 500-h oxidation, Cr_2O_3 and porous spinel appeared in the TGO on two types of the as-cold-sprayed coatings. However, the TGO formed on the LPPS MCrAlY coating with the surface recoated by splashed sputters was composed of Al_2O_3 and Cr/Ni oxides because of the increased surface areas and weakly adhered sputters on the coating surface. The content of spinel on the cold-sprayed NiCrAlY coating with a shot-peened surface was lower than that on the NiCrAlY coating with the as-cold-sprayed surface after 500-h oxidation. The Cr/Ni oxides grown at the surface of Al_2O_3 were attributed to the Ni, Cr elements diffusion in the Al_2O_3 scale and the Al depletion in the MCrAlY coating.

Acknowledgments

This study was financially supported by the National Basic Research Program of China (No. 2007CB707702), and the National Science Fund for Distinguished Young Scholars (No. 50725101).

References

1. A.G. Evans, D.R. Mumm, J.W. Hutchinson, G.H. Meier, and F.S. Pettit, Mechanisms Controlling the Durability of Thermal Barrier Coatings, *Prog. Mater. Sci.*, 2001, **46**(5), p 505-553
2. W.J. Brindley, Thermal Barrier Coatings, *J. Therm. Spray Technol.*, 1996, **5**(4), p 379-380
3. T. Strangman, D. Raybould, A. Jameel, and W. Baker, Damage Mechanisms, Life Prediction, and Development of EB-PVD Thermal Barrier Coatings for Turbine Airfoils, *Surf. Coat. Technol.*, 2007, **202**, p 658-664
4. Q. Zhang, C.-J. Li, Y. Li, S.-L. Zhang, X.-R. Wang, G.-J. Yang, and C.-X. Li, Thermal Failure of Nanostructured Thermal Barrier Coatings with Cold-Sprayed Nanostructured NiCrAlY Bond Coat, *J. Therm. Spray Technol.*, 2008, **17**(5-6), p 838-845
5. S. Ahmaniemia, P. Vuoristoa, T. Mäntylä, C. Gualco, A. Bonadei, and R. Di Maggio, Thermal Cycling Resistance of Modified Thick Thermal Barrier Coatings, *Surf. Coat. Technol.*, 2005, **190**, p 378-387
6. T. Vogt, B.A. Hunter, and J. Thornton, Structural Evolution of Thermal-Sprayed Yttria-Stabilized ZrO_2 Thermal Barrier Coatings with Annealing—A Neutron Diffraction Study, *J. Am. Ceram. Soc.*, 2001, **84**(3), p 678-680
7. S. Bose and J.D. Marcin, Thermal Barrier Coating Experience in Gas Turbine Engines at Pratt & Whitney, *J. Therm. Spray Technol.*, 1997, **6**(1), p 99-103
8. C.G. Levi, Emerging Materials and Processes for Thermal Barrier Systems, *Curr. Opin. Solid State Mater. Sci.*, 2004, **8**, p 77-91
9. A. Gil, V. Shemet, R. Vassen, M. Subanovic, J. Toscano, D. Naumenko, L. Singheiser, and W.J. Quadakkers, Effect of Surface Condition on the Oxidation Behavior of MCrAlY coatings, *Surf. Coat. Technol.*, 2006, **201**, p 3824-3828
10. A. Hesnawi, H.-F. Li, Z.-H. Zhou, S.-K. Gong, and H.-B. Xu, Effect of Surface Condition During Pre-Oxidation Treatment on Isothermal Oxidation Behavior of MCrAlY Bond Coat Prepared by EB-PVD, *Surf. Coat. Technol.*, 2007, **201**, p 6793-6796
11. N.P. Padture, M. Gell, and E.H. Jordan, Thermal Barrier Coatings for Gas-Turbine Engine Applications, *Science*, 2002, **12**(296), p 280-284
12. K.W. Schlichting, N.P. Padture, E.H. Jordan, and M. Gell, Failure Modes in Plasma-Sprayed Thermal Barrier Coatings, *Mater. Sci. Eng. A-Struct.*, 2003, **342**, p 120-130
13. F.-H. Yuan, Z.-X. Chen, Z.-W. Huang, Z.-G. Wang, and S.-J. Zhu, Oxidation Behavior of Thermal Barrier Coatings with HVOF and Detonation-Sprayed NiCrAlY Bondcoats, *Corros. Sci.*, 2008, **50**, p 1608-1617
14. F. Tang and J.M. Schoenung, Local Accumulation of Thermally Grown Oxide in Plasma-Sprayed Thermal Barrier Coatings with Rough Top-Coat/Bond-Coat Interfaces, *Scripta Mater.*, 2005, **52**, p 905-909
15. A.M. Karlsson, J.W. Hutchinson, and A.G. Evans, The Displacement of the Thermally Grown Oxide in Thermal Barrier Systems upon Temperature Cycling, *Mater. Sci. Eng. A*, 2003, **351**, p 244-257
16. S. Faulhaber, C. Mercer, M.-W. Moon, J.W. Hutchinson, and A.G. Evans, Buckling Delamination in Compressed Multilayers on Curved Substrates with Accompanying Ridge Cracks, *J. Mech. Phys. Solids*, 2006, **54**, p p1004-p1028
17. H.X. Zhu, N.A. Fleck, A.C.F. Cocks, and A.G. Evans, Numerical Simulations of Crack Formation from Pegs in Thermal Barrier Systems with NiCoCrAlY Bond Coats, *Mater. Sci. Eng. A*, 2005, **404**, p 26-32
18. U. Schulz, K. Fritscher, and A.E. Stahl, Cyclic Behavior of EB-PVD Thermal Barrier Coating Systems with Modified Bond Coats, *Surf. Coat. Technol.*, 2008, **203**, p 449-455
19. H.-B. Xu, S.-K. Gong, Y. Zhang, and C.-X. Zhang, Experimental and Computational Study on Hot Fatigue Process of Thermal Barrier Coatings by EB-PVD, *Intermetallics*, 2005, **13**, p 315-322
20. A. Gil, D. Naumenko, R. Vassen, J. Toscano, M. Subanovic, L. Singheiser, and W.J. Quadakkers, Y-rich Oxide Distribution in Plasma Sprayed MCrAlY-Coatings Studied by SEM with a Cathodoluminescent Detector and Raman Spectroscopy, *Surf. Coat. Technol.*, 2009, **204**, p 531-538
21. A. Rabiei and A.G. Evans, Failure Mechanisms Associated with the Thermally Grown Oxide in Plasma-Sprayed Thermal Barrier Coatings, *Acta Mater.*, 2000, **48**(15), p 3963-3976
22. M. Shibata, S. Kuroda, H. Murakami, M. Ode, M. Watanabe, and Y. Sakamoto, Comparison of Microstructure and Oxidation Behavior of CoNiCrAlY Bond Coatings Prepared by Different Thermal Spray Processes, *Mater. Trans.*, 2006, **47**(7), p 1638-1642
23. W.-R. Chen, X. Wu, B.R. Marple, D.R. Nagy, and P.C. Patnaik, TGO Growth Behaviour in TBCs with APS and HVOF Bond Coats, *Surf. Coat. Technol.*, 2008, **202**, p 2677-2683
24. Y. Li, C.-J. Li, G.-J. Yang, and L.-K. Xing, Thermal Fatigue Behavior of Thermal Barrier Coatings with the MCrAlY Bond Coats by Cold Spraying and Low-Pressure Plasma Spraying, *Surf. Coat. Technol.*, 2010, doi:10.1016/j.surfcoat.2010.08.144
25. Y. Li, C.-J. Li, Q. Zhang, G.-J. Yang, and C.-X. Li, Influence of TGO Composition on the Thermal Shock Lifetime of Thermal Barrier Coatings with Cold-Sprayed MCrAlY Bond Coat, *J. Therm. Spray Technol.*, 2010, **19**(1-2), p 168-177
26. Q. Zhang, C.-J. Li, C.-X. Li, G.-J. Yang, and S.-C. Lui, Study of Oxidation Behavior of Nanostructured NiCrAlY Bond Coatings Deposited by Cold Spraying, *Surf. Coat. Technol.*, 2008, **202**(14), p 3378-3384
27. P. Richer, M. Yandouzi, L. Beauvais, and B. Jodoin, Oxidation Behaviour of CoNiCrAlY Bond Coats Produced by Plasma, HVOF and Cold Gas Dynamic Spraying, *Surf. Coat. Technol.*, 2010, **204**(24), p 3962-3974
28. P. Richer, A. Zúñiga, M. Yandouzi, and B. Jodoin, CoNiCrAlY Microstructural Changes Induced During Cold Gas Dynamic Spraying, *Surf. Coat. Technol.*, 2008, **203**(3-4), p 364-371
29. W.-Y. Li, H.-L. Liao, C.-J. Li, G. Li, C. Coddet, and X.-F. Wang, On High Velocity Impact of Micro-Sized Metallic Particles in Cold Spraying, *Appl. Surf. Sci.*, 2006, **253**, p 2852-2862
30. M. Grujicic, C.L. Zhao, W.S. DeRosset, and D. Helfritch, Adiabatic Shear Instability Based Mechanism for Particles/Substrate Bonding in the Cold-Gas Dynamic-Spray Process, *Mater. Des.*, 2004, **25**, p 681-688
31. W.-Y. Li, C. Zhang, X.-P. Guo, C.-J. Li, H.-L. Liao, and C. Coddet, Study on Impact Fusion at Particle Interfaces and its Effect on Coating Microstructure in Cold Spraying, *Appl. Surf. Sci.*, 2007, **254**, p 517-526
32. G.-S. Huang, Deposition Properties of Cold-Sprayed CoNiCrAlY Coatings Prepared with Nitrogen Gas, *Proceedings of the 4th*

Asian Thermal Spray Conference, C.-J. Li and G.-J. Yang, Ed., Oct. 22-24, 2009 (Xi'an, China), 2009, p 366-369
33. D. Seo, K. Ogawa, Y. Suzuki, K. Ichimura, T. Shoji, and S. Murata, Comparative Study on Oxidation Behavior of Selected MCrAlY Coatings by Elemental Concentration Profile Analysis, *Appl. Surf. Sci.*, 2008, **255**, p 2581-2590
34. R. Chegroune, E. Salhi, A. Crisci, Y. Wouters, and A. Galerie, On the Competitive Growth of Alpha and Transient Aluminas During the First Stages of Thermal Oxidation of FeCrAl Alloys at Intermediate Temperatures, *Oxid. Met.*, 2008, **70**, p 331-337
35. Y.-S. Yi and J.-D. Zhang, Alumina Ceramic Material and Its Composite, Chemical Industry Press, 2001, p 93 (in Chinese)
36. M. Matsumoto, K. Hayakawa, S. Kitaoka, H. Matsubara, H. Takayama, Y. Kagiya, and Y. Sugita, The Effect of Pre-Oxidation Atmosphere on Oxidation Behavior and Thermal Cycle Life of Thermal Barrier Coatings, *Mater. Sci. Eng. A*, 2006, **441**, p 119-125
37. M. Matsumoto, T. Kato, K. Hayakawa, N. Yamaguchi, S. Kitaoka, and H. Matsubara, The Effect of Pre-Oxidation Atmosphere on the Durability of EB-PVD Thermal Barrier Coatings with CoNiCrAlY Bond Coats, *Surf. Coat. Technol.*, 2008, **202**(12), p 2743-2748
38. F. Tang, L. Ajdelsztajn, and J.M. Schoenung, Influence of Cryomilling on the Morphology and Composition of the Oxide Scales Formed on HVOF CoNiCrAlY Coatings, *Oxid. Met.*, 2004, **61**(3/4), p 219-238
39. M.S. Ali, S.H. Song, and P. Xiao, Degradation of Thermal Barrier Coatings Due to Thermal Cycling up to 1150 °C, *J. Mater. Sci.*, 2002, **37**, p 2097-2102
40. M. Dressler, M. Nofz, I. Dörfel, and R.S. Neumann, Influence of Sol-Gel Derived Alumina Coatings on Oxide Scale Growth of Nickel-Base Ssuperalloy Inconel-718, *Surf. Coat. Technol.*, 2008, **202**, p 6095-6102
41. Y.J. Su, R.W. Trice, K.T. Faber, H. Wang, and W.D. Porter, Thermal Conductivity, Phase Stability, and Oxidation Resistance of $Y_3Al_5O_{12}$ (YAG)/Y_2O_3-ZrO_2 (YSZ) Thermal-Barrier Coatings, *Oxid. Met.*, 2004, **61**(3-4), p 253-271
42. H. Yamano, K. Tani, Y. Harada, and T. Teratani, Oxidation Control with Chromate Pretreatment of MCrAlY Unmelted Particle and Bond Coat in Thermal Barrier Systems, *J. Therm. Spray Technol.*, 2008, **17**(2), p 275-283
43. P. Saltykov, O. Fabrichnaya, J. Golczewski, and F. Aldinger, Thermodynamic Modeling of Oxidation of Al-Cr-Ni Alloys, *J. Alloy. Compd.*, 2004, **381**, p 99-113
44. U. Dragos, M. Gabriela, B. Waltraut, and C. Ioan, Improvement of the Oxidation Behavior of Electron Beam Remelted MCrAlY Coatings, *Solid State Sci.*, 2005, **7**, p 459-464
45. M. Karadge, X. Zhao, M. Preuss, and P. Xiao, Microtexture of the Thermally Grown Alumina in Commercial Thermal Barrier Coatings, *Scripta Mater.*, 2006, **54**(4), p 639-644